Eur. J. Mech. B - Fluids 20 (2001) 489–510

S0997-7546(01)01126-8/REV

REVIEW ARTICLE

Turbulence and vortex structures in rotating and stratified flows

Claude Cambon

Laboratoire de Mécanique des Fluides et d'Acoustique, UMR 5509, École Centrale de Lyon, BP 163, 69131 Ecully cedex, France

(Received 22 February 2000; accepted 2 August 2000)

Abstract – Linear and nonlinear structuring effects caused by Coriolis force and/or buoyancy force/density stable stratification are surveyed and discussed in this article. Its main part, which reports on theoretical, experimental and numerical results, illustrates what can be explained from classic approaches to anisotropic homogeneous turbulence, taking advantage of the close relationship between 'two-point closures theories' and 'weakly nonlinear theories for wave turbulence'. The description including anisotropy allows the representation of linear and nonlinear interactions in terms of detailed eigenmodes of motion, like 'vortex' and 'waves', including the angular dependence of related scalar spectra and co-spectra in Fourier space. This anisotropic description is shown to be relevant to obtain precise indicators of the 'columnar' and 'pancake' structuring in physical space, by calculating for instance integral length scales for both different velocity components and different directions of two-point separations, vertical and horizontal. Additional effects of local forcing and confinement are investigated to understand the creation of coherent quasi-two dimensional vortices by pure rotation, from initially strongly three-dimensional, unstructured turbulence. Finally, stability analysis is briefly considered when the rotating and/or stratified flow consists of 'pre-existing' coherent large-scale vortices subject to three-dimensional disturbances. © 2001 Éditions scientifiques et médicales Elsevier SAS

turbulence / waves / vortices / rotation / stratification

1. Introduction

Effects of rotation on the structure of weak and developed turbulence present interest in industrial flows, while effect of stable density stratification and coupled effects stratification-rotation occur in geophysical flows. In these cases, the role of body forces (Coriolis, buoyancy) and mean gradients (density but not velocity) is subtle and difficult to model, since their linear dynamics consist of steady or oscillating modes of motion, the latter being linked to dispersive waves. By contrast with shear flows, there is no direct production of energy by linear effects, and the alteration of the structure of energy is essentially controlled by nonlinear interactions, such as resonant waves for instance.

This paper is firstly a survey of previous experimental, theoretical, and numerical approaches to rotating turbulence, without attempting to be exhaustive and likely being somewhat subjective. Since linear theory, such as 'Rapid Distortion Theory', and nonlinear two-point closure theory, such as anisotropic 'EDQNM', have given interesting guidelines for understanding dynamics of rotating turbulence, and moreover have often suggested key quantities to investigate in experimental and numerical experiments, these theories were generalized to allow application to the dynamics of stratified and rotating-stratified turbulence. We also took advantage of the close relationship of our 'anisotropic closures' to 'wave turbulence' weakly nonlinear theories, which are the object of an increasing number of works [1–4]. This theoretical background is the main theme throughout this article. Stability of coherent structures in rotating/stratified field is also touched upon, in connection with columnar structuring/layering. From a more physical viewpoint, 'pancake dynamics'

E-mail address: cambon@mecaflu.ec-lyon.fr (C. Cambon).

and the 'geostrophic adjustment' are at the heart of a timely debate among geophysicists, engineers, and mathematicians.

The paper is organised as follows. Background equations for rotating and stratified flows are given in section 2, with a preliminary discussion of wave regimes, and anisotropic structuring connected with linear and nonlinear effects. The case of homogeneous rotating turbulence is extensively treated in section 3, and is the most detailed. Additional effects of confinment and local forcing are presented in section 4, using DNS results and qualitative comparisons with a typical experiment (Hopfinger et al. [5]). Sections 5 and 6 deal with pure stratified and rotating-stratified turbulence, respectively.

2. Background for linear and nonlinear dynamics

Navier–Stokes equations with the Boussinesq approximation in a rotating frame are

$$(\partial_t + \mathbf{u}\cdot\nabla)\mathbf{u} + 2\Omega\mathbf{n}\times\mathbf{u} + \nabla p - \nu\nabla^2\mathbf{u} = \mathbf{n}b, \tag{1}$$

$$(\partial_t + \mathbf{u}\cdot\nabla)b - \chi\nabla^2 b = -N^2\mathbf{n}\cdot\mathbf{u}, \tag{2}$$

$$\nabla\cdot\mathbf{u} = 0, \tag{3}$$

where $\mathbf{u}$, p and b are the fluctuating velocity, pressure (divided by mean density of reference), and buoyancy force intensity, respectively. $\mathbf{n}$ denotes the vertical unit upward vector with which are aligned both the gravitational acceleration, $\mathbf{g} = -g\mathbf{n}$, and the angular velocity of the rotating frame $\mathbf{\Omega} = \Omega\mathbf{n}$. The buoyancy force is related to the fluctuating temperature field τ by $\mathbf{b} = -\mathbf{g}\beta\tau$, through the coefficient of thermal expansivity β, and the temperature stratification is characterized by the vertical gradient γ. Using b instead of τ in the first two equations above yields introducing the Brûmt–Wäisälä frequency N only as the characteristic frequency of buoyancy-stratification, with $N = \sqrt{\beta g\gamma}$. Hence the linear operators in equations (1) and (2) display the two frequencies N and 2Ω, having the ratio $B = 2\Omega/N$. Given the symmetry of these equations (axisymmetry around the axis $\mathbf{n}$), the direction parallel to, with subscript $\|$, and the direction perpendicular to $\mathbf{n}$, with subscript $\perp$, will be extensively used from now on for vectorial quantities. Without loss of generality the fixed frame of reference will be chosen so that $n_i = \delta_{i3}$ if tensorial notations are needed, with $u_3 = u_\|$ being for instance the vertical, or axial, velocity component.

2.1. Internal gravity waves and 'vortex' mode in pure stratified case

The linear inviscid limit for the non rotating case, $\Omega = 0$, $N \neq 0$, is firstly recalled as follows. The linear limit is obtained by discarding the advection term in both equations (1) and (2). In addition, the inviscid limit $\nu = \chi = 0$ is considered. Without the pressure term in (1), the resulting system of equations (1) and (2) admit sinusoidal solutions, with frequency N, for vertical velocity component u_3 and buoyancy term b, with opposite phase. Of course, these pressureless solutions are not valid in the general case, and the pressure term is needed for satisfying the solenoidal constraint (3). The pressure term is responsible for a coupling between horizontal and vertical velocity components, and for the anisotropic dispersion law of internal gravity waves. The last effect is essential since the pressureless linearised equations admit 'oscillating' solutions, but not really 'propagating waves' solutions. Eliminating velocity in the system of equations (1)–(3) yields

$$\partial_t^2(\nabla^2 p) + N^2\nabla_\perp^2 p = 0, \tag{4}$$

where $\nabla_\perp^2$ and $\nabla_\parallel^2$ (see below) denote the horizontal part and the vertical part, respectively, of the Laplacian operator. An illustration of the specific wave properties of internal waves is given in *figure 1* (which displays the work of [6–8]), when the stably stratified flow with uniform B-W frequency N is locally subjected to a harmonic forcing of given frequency σ_0. The rays in the figure correspond to isophase surfaces emanating from the small forced zone, and they are visualized through the strong shear between them. This typical cross-shaped structure induced by gravity waves appears for $\sigma_0 < N$. In accordance with the normal form of forced solutions $p = \mathrm{e}^{-\imath\sigma_0 t}\mathcal{P}(\mathbf{x})$, the previous pressure equation becomes $\sigma_0^2\nabla_\parallel^2\mathcal{P} + (\sigma_0^2 - N^2)\nabla_\perp^2\mathcal{P} = 0$, showing a change from elliptic to hyperbolic type when σ_0 crosses the value N by decreasing values. In addition, the pressure equation exhibits the typical dispersion law

$$\sigma_k = \pm N\frac{k_\perp}{k} = \pm N\sin\theta_k \tag{5}$$

with $k = \sqrt{k_1^2 + k_2^2 + k_3^2}$, $k_\perp = \sqrt{k_1^2 + k_2^2}$, and θ_k being the angle of $\mathbf{k}$ with the vertical direction, for solutions under the form of plane waves $p = P\exp[\imath(\mathbf{k}\cdot\mathbf{x} - \sigma t)]$. The angle of the rays in the figure can be closely

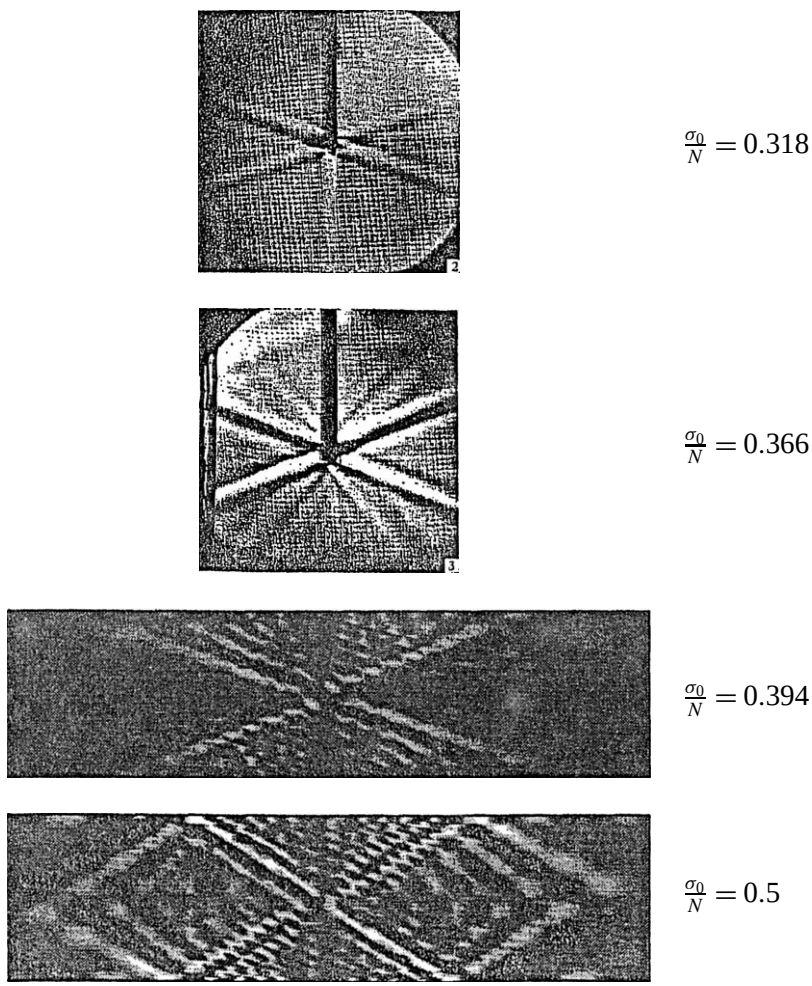

Figure 1. Cross-shaped structures generated by a point forcing through internal gravity waves. Courtesy Mowbray and Rarity [6] (experiment, top) and Lollini [7], (DNS, bottom).

related to the angle given by the resonance condition, $\sigma_0 = \sigma_k = \pm N \sin\theta_k$, in which $\mathbf{k}$ is readily assumed to be normal to the thick rays, interpreted as isophase surfaces, in *figure 1*. In the general unforced case where pressure disturbances consist of a dense spectrum of modes with different angles θ_k, different frequencies $|\sigma|$ are permitted, ranging from 0 (for vertical wave vectors) to N (for horizontal wave vectors).

This analysis can be readily extended to the velocity field, under the form of plane waves. It appears that the solenoidal part of the horizontal field is unaffected by the wave regime and remains constant in the linear inviscid limit: it corresponds to the 'vortex', or potential vorticity (PV hereinafter), part (see Riley et al. [9], Riley and Lelong [10]). Only the complementary part is involved in the wave regime in a way similar to the pressure. Hence, complete linear solutions for velocity in term of plane waves are

$$u_i(\mathbf{x}, t) = \int \exp(\imath \mathbf{k} \cdot \mathbf{x}) \left[A_i^0 + A_i^1 \exp(\imath \sigma_k t) + A_i^{-1} \exp(-\imath \sigma_k t) \right] \mathrm{d}^3\mathbf{k}, \tag{6}$$

where the $A_i^\varepsilon, \varepsilon = 0, \pm 1$ are projections of the initial disturbance field onto the three eigenmodes, one steady – the 'vortex' mode – $\mathbf{N}^0$ and two 'wavy' $\mathbf{N}^{\pm 1}$ (see Appendix). From now on, σ_k will denote the 'absolute value of the dispersion' law. Detailed equations for pure stratification and rotation-stratification will be given or recalled in the next sections.

2.2. Towards the general (rotating + stratified) case

Equation (6) is sufficient for preliminary qualitative discussion of linear and nonlinear effects in the general case. The general case of rotation-stratification yields linear inviscid solutions of the same type as (6), slightly modifying the definition of steady and wavy modes (see Appendix), and changing the dispersion law (5) into

$$\sigma_k = \sqrt{N^2 \sin^2\theta_k + 4\Omega^2 \cos^2\theta_k}. \tag{7}$$

It is important to notice that the case of pure rotation, $N = 0$, is singular in the sense that the steady mode, which is linked to $\mathbf{A}^0$ in (6), vanishes for velocity. In this case, let us point out the essential difference between a steady mode which is defined for any direction of $\mathbf{k}$ and the steady limit of the wavy mode when $\sigma_k = 0$ ($\cos\theta_k = 0$ or 2D mode for pure rotation).

The general method for obtaining linear solutions in 3D Fourier space is completely consistent with the previous analysis with equations of type (6). Pressure fluctuation in (1) is removed from consideration by using a local frame in the plane normal to the wave vector [11], taking advantage of (3), so that the problem in five components (u_1, u_2, u_3, p, b) in physical space is reduced to a problem in three components, two solenoidal velocity components and a component for b, in Fourier space. For mathematical convenience, as in Cambon [12] and Godeferd and Cambon [13], the velocity-temperature field in three components is finally gathered into a single vector $\mathbf{v}$, whose 3D Fourier transform, denoted by a 'hat' $\widehat{(\,)}$, can be written as

$$\widehat{\mathbf{v}} = \widehat{\mathbf{u}} + \imath \frac{1}{N} \widehat{b} \frac{\mathbf{k}}{k}. \tag{8}$$

(A similar three-component term, denoted $\mathbf{W}_K$, is extensively used in Riley and Lelong [10], p. 626, but it is not a true vector in contrast to $\widehat{\mathbf{v}}$, see the Appendix for detailed relationship.) The scaling of the contribution from buoyancy force allows to define twice the total energy spectral density as

$$\widehat{v}_i^* \widehat{v}_i = \widehat{u}_i^* \widehat{u}_j + N^{-2} \widehat{b}^* \widehat{b}. \tag{9}$$

Without stratification, N^{-1} has to be replaced by another time scale τ_0 in the equation (8), but coupling between velocity and buoyancy fields vanishes in this case.

Looking only at inviscid linear solutions (or 'Rapid Distortion Theory', RDT hereinafter [14–16]) for two-point and single-point velocity or buoyancy second-order correlations, the following results can be predicted without detailed calculations:

- inviscid RDT solutions are derived from (6) and (8) for second-order spectral tensors, which are related to $\langle \widehat{u}_i^* \widehat{u}_j \rangle$, or $\langle \widehat{v}_i^* \widehat{v}_j \rangle$. They consist of sums of steady and oscillating terms, the frequency of oscillations being directly connected to the dispersion law of internal waves. Such solutions are completely reversible;
- after integration over **k**-space, including averaging over all directions, oscillating terms for spectral tensors yield 'damped' oscillations. This damping effect, called 'phase-mixing' in [17], physically reflects the 'anisotropic dispersivity' of inertio-gravity waves. It cannot appear for $N = 2\Omega$, or for particular initial data at $N \neq 2\Omega$, such as the equipartion case considered for nonlinear applications in [13]). The fact that some terms in $\widehat{u}_i^* \widehat{u}_j$ are conserved after integration, such as those coming from $A_i^{0*} A_j^0$ from (6), whereas other ones are damped, such as those from $A_i^{0*} A_j^{\pm 1}$, explains the change of anisotropy over time for all single-point correlations. This change is completely related to the initial distribution in terms of steady and wavy modes.

Except for the anisotropisation of 'two-time' single-point correlations, the linear limit exhibits no interesting creation of structural anisotropy. This creation is connected to two-dimensionalisation in rotating turbulence or horizontal layering tendency in the stably stratified case. In other words, RDT only alters phase dynamics, and conserves exactly the spectral density of typical modes (full kinetic energy for the rotating case, total energy and 'vortex', or PV, energy for the stably stratified case), so that two-dimensionalisation or 'two-componentalization' (horizontal layering), which affect the distribution of this energy, are typically nonlinear effects. In Godeferd and Cambon [18], RDT results begin to be compared with the results of a full DNS, in order to have the definite answer on what is linear (given by RDT) and what is nonlinear (only given by DNS) in the rotating + stratified case. In addition to such numerical comparisons, which exhibit the typically nonlinear effects, RDT has another role, not only to provide the reference for pure linear dynamics: the eigenmodes of the linear regime, derived from RDT, form a useful basis for expanding the fluctuating velocity-temperature field, even when nonlinearity is present, and nonlinear interactions can be evaluated and discussed in terms of triadic interactions between these eigenmodes. Accordingly, the complete anisotropic description of two-point second order correlations can be related to spectra and co-spectra of these eigenmodes. As an illustration, the complete equations (1)–(3) become

$$\left(\partial_t + \nu k^2 + \imath \varepsilon \sigma_k\right) \xi_\varepsilon(\mathbf{k}, t) = \sum_{\varepsilon', \varepsilon'' = 0, \pm 1} \int_{p+q=k} m_{\varepsilon \varepsilon' \varepsilon''}(\mathbf{k}, \mathbf{p}) \xi_{\varepsilon'}(\mathbf{p}, t) \xi_{\varepsilon''}(\mathbf{q}, t) \, \mathrm{d}^3\mathbf{p} \tag{10}$$

with $\varepsilon = 0, \pm 1$, after projection onto the normal modes of **v** in Fourier space.

The basis of eigenmodes (see the appendix) is used to express $\widehat{\mathbf{v}}$ as

$$\widehat{\mathbf{v}} = \sum_{\varepsilon = 0, \pm 1} \xi^\varepsilon \mathbf{N}^\varepsilon, \tag{11}$$

with

$$\xi^\varepsilon = \widehat{\mathbf{v}} \cdot \mathbf{N}^{-\varepsilon}, \quad \varepsilon = 0, \pm 1. \tag{12}$$

For the sake of simplicity, the Prandtl number is chosen equal to one in (10). If not, laminar diffusion affects the very definition of eigenmodes and dispersion frequencies [15]. This equation yields the exact separation

between the linear, diagonal, operator in the left-hand side, and the triadic nonlinear operator in the right-hand side. Briefly looking at turbulence modeling, it is necessary to distinguish the nonlocal problem, which is mainly due to the relationship between pressure and velocity fluctuation, and the nonlinear problem. Although purely linear theory closes the equations without further ado and simplifies mathematical analysis, it is rather limited in its domain of applicability, ignoring as it does all interactions of turbulence with itself, including the physically important cascade process. Multi-point turbulence models which account for nonlinearity via closure lead to moment equations with a well-defined linear operator and nonlinear source terms. (see Cambon and Scott [16] for a review).

One may nonetheless conjecture that linear effects continue to be important in structuring the turbulence, although linear theory itself no longer gives a precise description. It is not possible to discuss in a general way the nonlinear problem, which is very complex and multiform, particularly when the turbulence is subjected to effects of mean gradients and/or body forces. This problem will be mainly illustrated by the effects of pure rotation in the next section.

3. Pure rotating homogeneous turbulence

3.1. The transition from 3D *to* 2D *structure: a nonlinear mechanism*

A rotating fluid leads to inertial waves (Greenspan [8]) whose linearised properties are well-understood and whose amplitudes provide a set of variables for which the linear behaviour is particularly simple. As for the stably stratified case, local harmonic forcing of frequency σ_0 can generate characteristic 'St Andrew cross' structures in a rotating tank, provided $\sigma_0 < 2\Omega$. The angle of the rays can be given by the resonance condition $\sigma_0 = \sigma_k$, in which

$$\sigma_k = \pm 2\Omega \frac{k_\parallel}{k} = 2\Omega \cos\theta_k \tag{13}$$

is the dispersion law of inertial waves, with $k_\parallel$ the component of $\mathbf{k}$ along the rotation axis. Linear theory describes rotating turbulence as a combination of inertial waves, which interact when nonlinearity is allowed for via selective resonant transfers whose origin is best understood with linear theory as a background.

In the absence of mean gradients in the rotating frame, the vorticity $\boldsymbol{\omega} = \nabla \times \mathbf{u}$ is governed by

$$\frac{\partial \omega_i}{\partial t} - 2\Omega_j \frac{\partial u_i}{\partial x_j} = \frac{\partial u_i}{\partial x_j}\omega_j - u_j \frac{\partial \omega_i}{\partial x_j} + \nu \frac{\partial^2 \omega_i}{\partial x_j \partial x_j}. \tag{14}$$

Only the linear second term in the left-hand side explicitly involves the angular velocity of the rotating frame of reference. Nonlinear and viscous terms are gathered on the right-hand side.

In agreement with the Proudman theorem, a two dimensional state, or $\Omega_j \frac{\partial u_i}{\partial x_j} = 0$, is found in the limit of low Rossby number, high Reynolds number, and slow motions. The first two conditions yield neglecting right-hand side terms, whereas the last one amounts to neglecting the temporal derivative. It is important to point out that the Proudman theorem says only that the 'slow manifold' of the linear regime necessarily is the 'two-dimensional manifold', but it cannot predict the transition from 3D to 2D structure, which is a typically nonlinear and unsteady process (see Cambon et al. [19], for a survey).

For unforced, unbounded, turbulent field, the linear limit of the unsteady system of equations (1)–(3) or (10) consists of superposition of inertial waves (for u_i, ω_i, p, ...), of the form (6) with $A_i^0 = 0$, and σ_k given by (13). In agreement with this dispersion law, the slow manifold is recovered as the wave plane orthogonal

to the rotation axis, for $k_\parallel = 0$ which corresponds to $\partial/\partial x_\parallel = 0$ in physical space. However, the linear regime conserves the spectral density of energy, or $\widehat{u}_i^* \widehat{u}_i$, so that the transition from 3D to 2D turbulence must be interpreted as an angular drain of energy from oblique wavevectors towards the waveplane $k_\parallel = 0$, energy drain which is mediated by nonlinear interactions.

This tendency, which is a partial two-dimensionalisation induced by 'nonlinear' interactions, has been extensively studied in homogeneous turbulence, using experimental (Jacquin et al. [20], and references therein), theoretical and DNS/LES high resolution results ([21,19]). In physical space, the partial two-dimensionalisation is reflected by the rise of anisotropic relationship for the integral lengthscales $L_{ij}^{(n)}$ (definition further recalled in equation (22)), with dominant increase of axially separated integral ones ($n = 3$). The Reynolds stress tensor anisotropy remains weak, with a significant dominance of the axial component, or $\langle u_\parallel^2 \rangle = \langle u_3^2 \rangle > \langle u_1^2 \rangle = \langle u_2^2 \rangle = \langle u_\perp^2 \rangle$. This illustrates the essential difference between the two-dimensional limit, or $\partial/\partial x_\parallel = 0$, and the two-component limit, or $u_\parallel = 0$. In addition, anisotropic features linked to the two-dimensionalisation process were shown to be triggered at a 'macro-Rossby number' $Ro^L = u'/(2\Omega L_{33}^{(3)})$ close to one. Studies of temporal evolution of initially isotropic turbulence at high Rossby number ($Ro_L > 1$) display an 'intermediate' range of Rossby numbers, which is delineated by $Ro_L < 1$ and $Ro^\omega = \omega'/(2\Omega) \sim u'/(2\Omega\lambda) > 1$, for anisotropisation effects, the last Rossby number being a 'micro-Rossby' number, with λ a typical Taylor micro-scale. The

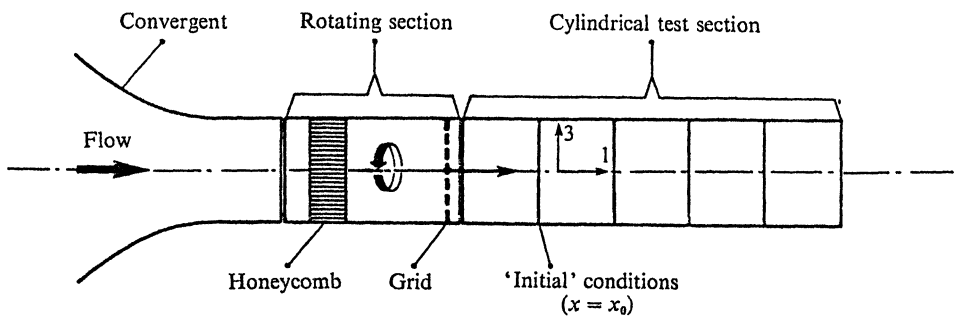

Schematic of the experimental set-up (ONERA).

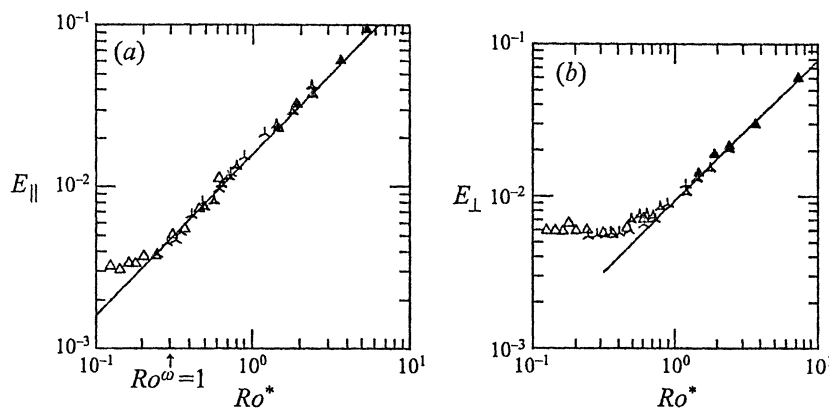

Evolution of (a) vertical non-dimensional energy $E_\parallel = E_v^v$ and (b) horizontal non-dimensional (i.e. divided by ΩUM^2) energy $E_\perp = E_h^v$. (Experiment by Jacquin.)

Figure 2. Experimental facility and typical results. The axes labeled 1 and 3 on the top sketch (experiment) have to be reversed to correspond to the ones used throughout the paper. $E_\parallel = \langle u_3^2 \rangle L_{33}^{(3)}$, $E_\perp = \langle u_1^2 \rangle L_{11}^{(3)} = \langle u_2^2 \rangle L_{22}^{(3)}$ (see equation (22)), and $Ro^* = \sqrt{\langle u_3^2 \rangle}/(2\Omega L_{33}^{(3)})$. See Jacquin et al. [20].

experimental facility used by Jacquin et al. [20]) is sketched in *figure 2* (top), together with typical results (bottom).

3.2. Wave turbulence and closure theories

Using (10), the 'rapid distortion', or equivalently the 'linear inviscid' limit is simply

$$\xi_\varepsilon(\mathbf{k},t) = \exp\bigl[\imath\varepsilon\sigma_k(t)\bigr]\xi_\varepsilon(\mathbf{k},0), \quad \varepsilon = \pm 1, \tag{15}$$

instead of $\widehat{v}_i(\mathbf{k},t) = G_{ij}(\mathbf{k},t,t_0)\widehat{v}_j(\mathbf{k},t_0)$ (general RDT solution, without convection, see [16]). Replacing the initial data at fixed $t_0 = 0$ in (15) by a new unknown variable, say a_ε, so that

$$\xi_\varepsilon(\mathbf{k},t) = \exp[\imath\varepsilon\sigma_k t]a_\varepsilon(\mathbf{k},t), \quad \varepsilon = \pm 1, \tag{16}$$

an equation for a_ε is readily derived from (10). Using the above transformation (16) (which amounts to the 'Poincaré transformation' used by [1] in the case of pure rotation), the nonlinear dynamics of a_ε is easily shown to be

$$\dot{a}_\varepsilon = \sum_{\varepsilon',\varepsilon''=\pm 1} \int_{k+p+q=0} \exp\bigl[\imath(\varepsilon\sigma_k + \varepsilon'\sigma_p + \varepsilon''\sigma_q)t\bigr] m_{\varepsilon\varepsilon'\varepsilon''}(\mathbf{k},\mathbf{p}) a^*_{\varepsilon'}(\mathbf{p},t) a^*_{\varepsilon''}(\mathbf{q},t)\,\mathrm{d}^3\mathbf{p}, \quad \varepsilon = \pm 1. \tag{17}$$

Time integrating the above equation, the following 'resonance operator' (see also Rubinstein [22]) is exhibited

$$\int \exp\bigl[\imath(\varepsilon\sigma_k + \varepsilon'\sigma_p + \varepsilon''\sigma_q)(t-t')\bigr]\phi(t,t')\,\mathrm{d}t'$$

in which ϕ holds for the quadratic contribution of 'slow' amplitudes, and is assumed to vary slowly with $t - t'$. Indeed, the zero value of the phase of the above kernel characterises the resonant condition, and the simultaneous conditions

$$\varepsilon\sigma_k + \varepsilon'\sigma_p + \varepsilon''\sigma_q = 0 \quad \text{with } \mathbf{k}+\mathbf{p}+\mathbf{q} = \mathbf{0} \tag{18}$$

give the resonant surfaces. Different works have been carried out in the case of 'weak' wave turbulence [1–4,22], including an asymptotic analysis in the vicinity of resonant surfaces in order to capture some 'slow' dynamics at leading order. Of course, this pattern is generic and can be encountered in other wave-turbulence contexts, changing only the dispersion law σ_k and/or the interaction matrix $m_{\varepsilon\varepsilon'\varepsilon''}$ in (10) and (17), but other mechanismes can render triadic wave resonance an irrelevant effect. Firstly, triple resonance can be forbidden by the dispersion law itself or by geometric constraints. This is often the case in plasma physics, or in the limit of rotating shallow waters. In these cases, the leading order which is relevant for slow nonlinear motion is the fourth one, and resonant quartets have to be considered. The debate triad-quartets is too controversial, at least in the cases considered herein, to be objectively reported here (see Smith and Waleffe [23] for rotating turbulence in both cubic and flattened boxes). Another, simpler, situation occurs when the basis of eigenmodes includes a non wavy mode. It is the case with the 'vortex', or 'potential vorticity', or 'quasi-geostrophic' mode involved in the stratified and rotating-stratified cases. Note that the two eigenmodes are wavy in (11) ($\varepsilon = \pm 1$ only) for pure rotation, and correspond to the 'helical modes' extensively used to analyse triadic interactions (e.g. [24,25, 19]), so that the stationary linear mode is singular. It does not correspond to the generic mode associated with $\varepsilon = 0$, only occuring when stratification is present, but corresponds to 'degenerated' wavy modes ($\varepsilon = \pm 1$), in the limit of vanishing frequency in (13).

Going back to the case of pure rotation without geometric constraints (such as flattened boxes), it is clear that the transition 3D–2D should be reflected in spectral space by an angular drain of spectral energy from linear unsteady wavy modes ($k_\parallel/k \neq 0$) towards the linear steady one ($k_\parallel/k = 0$). In addition, this angular drain should involve nonlinear interactions, so that only an unsteady and nonlinear approach can explain this transition. At small Rossby number, the long-time behaviour is dominated by near-resonant interactions, and a qualitative analysis of Waleffe [25] has shown how resonant interactions can concentrate energy towards the 2D manifold (see also Smith and Waleffe [23]).

It is possible to directly construct equations for 'slow' amplitude square and cross-correlations, or $\langle a_+^* a_+ \rangle$, $\langle a_-^* a_- \rangle$, $\langle a_+^* a_- \rangle$, from the above equations (10), (17). These quantities are kept constant in the 'RDT' limit, whereas the nonlinear terms responsible for their slow evolution are constructed, using either asymptotic developments of weak wave-turbulence or suitably generalized two-point closures. In order to connect that with classic turbulence theory, we will proceed in a slightly different way, by considering a fully anisotropic second-order spectral tensor and related transfer tensor.

The second-order spectral tensor $\Phi_{ij}(\mathbf{k}, t)$ is the Fourier transform of the two-point covariance matrix $\langle u_i(\mathbf{x}, t) u_j(\mathbf{x}', t) \rangle$, or

$$\left\langle \widehat{u}_i^*(\mathbf{p}, t) \widehat{u}_j(\mathbf{k}, t) \right\rangle = \Phi_{ij}(\mathbf{k}, t) \delta(\mathbf{k} - \mathbf{p}), \tag{19}$$

and its more general expression for homogeneous anisotropic turbulence is [26,19,16]

$$\Phi_{ij} = \begin{pmatrix} 0 & 0 & 0 \\ 0 & e + Z_r & Z_i - \imath \mathcal{H}/k \\ 0 & Z_i + \imath \mathcal{H}/k & e - Z_r \end{pmatrix} \tag{20}$$

using an orthonormal frame of reference, associated with polar-spherical coordinates (k, θ, φ) of $\mathbf{k}$ in Fourier space, as the Craya–Herring decomposition for the velocity field (see Appendix). Hence Φ_{ij} can be expressed as a sum of different contributions, in terms of the scalars e (energy spectrum), Z (polarisation anisotropy), with $Z = Z_r + \imath Z_i$ complex, and $\mathcal{H}$ (helicity spectrum), which all depend on $\mathbf{k}$. Isotropic turbulence is characterized by $e(k, \theta, \varphi, t) = E(k)/(4\pi k^2)$, $Z = \mathcal{H} = 0$, so that the real part of Φ_{ij}, which is involved in classic one-point correlations, involve e and Z contributions as follows

$$\mathrm{Re}(\Phi_{ij}) = \underbrace{\frac{E(k)}{4\pi k^2} P_{ij}}_{\text{Pure isotropic part}} + \underbrace{\left(e(k, \theta, \phi) - \frac{E(k)}{4\pi k^2} \right) P_{ij}}_{\text{Directional anisotropy}} + \underbrace{\mathrm{Re}(Z N_i N_j)}_{\text{Polarisation anisotropy}} \tag{21}$$

(see [19] for details, Re denotes the real part of a complex quantity, $P_{ij} = \delta_{ij} - k_i k_j / k^2$ is the classic projection operator, and $N_i = e_i^{(2)} - \imath e_i^{(1)}$ denotes the helical mode). It is clear from the above equation that the anisotropy is twofold. A lessening of dimensionality is only reflected by a nonzero value of the second term. Indeed, the directional anisotropy, which is expressed by a departure of e from a spherical equidistribution, is extreme in a pure two-dimensional state, where e is concentrated onto the plane $k_\parallel = 0$. From this viewpoint, the trend towards two-dimensionality (with e tending to concentrate near the plane $k_\parallel = 0$) in rotating turbulence has nothing to do with the trend towards the collapse of vertical motion (with e concentrating along the axis $k_\perp = 0$) encountered in stably stratified turbulence. (In agreement with the notation used throughout this article, $k_\parallel$ denotes the axial, or vertical, component of the vector $\mathbf{k}$, whereas $k_\perp$ is the transverse, or horizontal, component.)

Starting from (21), all the classic one-point correlations can be obtained and thus analysed in terms of both directional and polarisation anisotropies, including the Reynolds stress tensor, the vorticity correlation tensor

and other quantities. Among them, the integral length scales $L_{ij}^{(n)}$, related to different velocity correlations (subscripts i, j) which are separated along different directions (superscript n), give invaluable information.

$$\langle u_i u_j \rangle L_{ij}^{(n)} = \int_0^\infty \langle u_i(\mathbf{x}, t) u_j(\mathbf{x} + r\mathbf{s}^{(n)}, t) \rangle \, \mathrm{d}r = \pi \iint \Phi_{ij}|_{k_n=0} \, \mathrm{d}^2\mathbf{k} \tag{22}$$

with $s_i^{(n)} = \delta_{in}$. Typical products of Reynolds Stress components and integral length scales are shown on *figure 2* (bottom). In agreement with directional dependence and polarisation at the finest level of description (21), the integral length scale related to transverse velocity components ($i = j = 1, 2$) and axial ($n = 3$) separation is enhanced with respect to all the other components $L_{ij}^{(n)}$, whereas the Reynolds stress tensor is hardly anisotropic, with only a slight dominance of its axial component. The latter results were obtained by different approaches, with experimental measurements (see again *figure 2*), nonlinear closure models (see below), and high resolution DNS and LES (see [21,19]), which allow the development of axial integral length scales without interference with periodic boundary conditions.

The set $e, Z, \mathcal{H}$ is governed by the following system of equations

$$\left(\frac{\partial}{\partial t} + 2\nu k^2\right) e = T^{(e)}, \tag{23}$$

$$\left(\frac{\partial}{\partial t} + 2\nu k^2 + 4\imath \cos\theta_k\right) Z = T^{(Z)}, \tag{24}$$

$$\left(\frac{\partial}{\partial t} + 2\nu k^2\right) h = T^{(h)} \tag{25}$$

in which the right-hand sides reflect nonlinear transfer terms. Of course, the set $(e, Z, \mathcal{H})$ is immediately derived from the set of amplitude squares $\langle a_+^* a_+ \rangle$, $\langle a_-^* a_- \rangle$, $\langle a_+^* a_- \rangle \mathrm{e}^{-4\imath \cos\theta_k t}$ through linear combination (see [19]), and the generalized transfer terms $T^{()}$ are cubic in terms of these amplitudes.

In the general derivation of EDQN (Eddy Damped Quasi Normal), detailed anisotropy is preserved, and the structure of linear propagators is an essential ingredient. The complete equation (see Cambon and Scott [16], section 3) is not recalled for the sake of brevity. A complete closure of generalized transfer terms (T^e, T^z, T^h) in term of $(e, Z, \mathcal{H})$ is eventually derived using the decomposition (20) and the following Kraichnan 'response tensor'

$$G_{ij}^{QN} = \mathrm{Re}\big[N_i N_j^* \exp(\imath\sigma_k(t - t'))\big] \exp\big[-\mu_k(t - t')\big] \tag{26}$$

in which the viscous + eddy damping term μ_k has to be specified, or is governed by additional dynamical equations in more complex DIA or TFM versions. In the case of strong rotation, its role is only to ensure suitable convergence of temporal integrals, and its shape is unimportant, as we will discuss further. The final step in applying the procedure is the so-called 'markovianization'. In our context, this amounts to separating in the integrands terms considered as rapidly evolving and terms considered as slowly evolving. Only in the latter the non-instantaneous dependency with respect to the past time t' is reduced to an instantaneous dependency, making $t' = t$. The first non-trivial application of this procedure to wave-turbulence was called EDQNM2. Its advantage was to exhibit a generic closure relationship, for instance

$$T^{(e)} = \sum_{\varepsilon,\varepsilon',\varepsilon''=\pm 1} \int_{k+p+q=0} \frac{S^{QN}(\varepsilon\mathbf{k}, \varepsilon'\mathbf{p}, \varepsilon''\mathbf{q})}{\mu_k + \mu_p + \mu_q + \imath(\varepsilon\sigma_k + \varepsilon'\sigma_p + \varepsilon''\sigma_q)} \, \mathrm{d}^3\mathbf{p} \tag{27}$$

in which the imaginary term in the denominator naturally appears, as in (17), through the three-fold product of Green's functions (26). $T^{(e)}$ is mainly responsible for the angular drain of kinetic energy, which tends to condensate this energy towards the horizontal wave plane. The subsequent angular-dependent shape of $e(k, \cos\theta_k, t)$, which is nonlinearly created by pure rotation from pure isotropic initial data $e(k, 0) = E(k)/(4\pi k^2)$, is shown in *figure 3*, with results from both EDQNM2 model and high-resolution LES. The angular-dependent spectral shape, and, to a lesser extent, the polarisation of the spectral energy in the horizontal wave-plane, in (21), underly all the observed anisotropic features in physical space, as for the integral length scales and Reynolds stress components given by (22).

Only recently, it was shown that the treatment of the 'rapid' phase in the oscillating term Z was not consistent with a systematic separation rapid-slow underlied by (16) and its statistical moments up to the third order, and an improved version, EDQNM3, was constructed. Even if the two versions yield similar numerical results in rotating turbulence started with almost isotropic initial data, realizability is not ensured by EDQNM2 for any initial data, and localized lack of realizability were exhibited in the stably stratified case (van Haren [14]). As a bonus, a realisable, simplified asymptotic model AQNM is being derived from the EDQNM3 version (Godeferd et al. [27]) in the limit $\mu_k \ll \Omega$. This model gives the opportunity to investigate the limit of very small Rossby numbers, very high Reynolds, and very long time, limit which cannot be captured by standard pseudo-spectral DNS, and even by standard numerical calculations of discretized EDQNM2-3 versions.

Going back to experimental and numerical (more or less classic DNS-LES) experiments, which only deal with short times and moderate Reynolds numbers, they confirm that the nonlinear tendency to create columnar structures is very subtle and cannot yield to well organised arrays of 2D vortices. In an actual experiment or – explicitly inhomogeneous – numerical simulation, however, the forcing and/or the presence of solid boundaries can enforce the creation of such organised vortices.

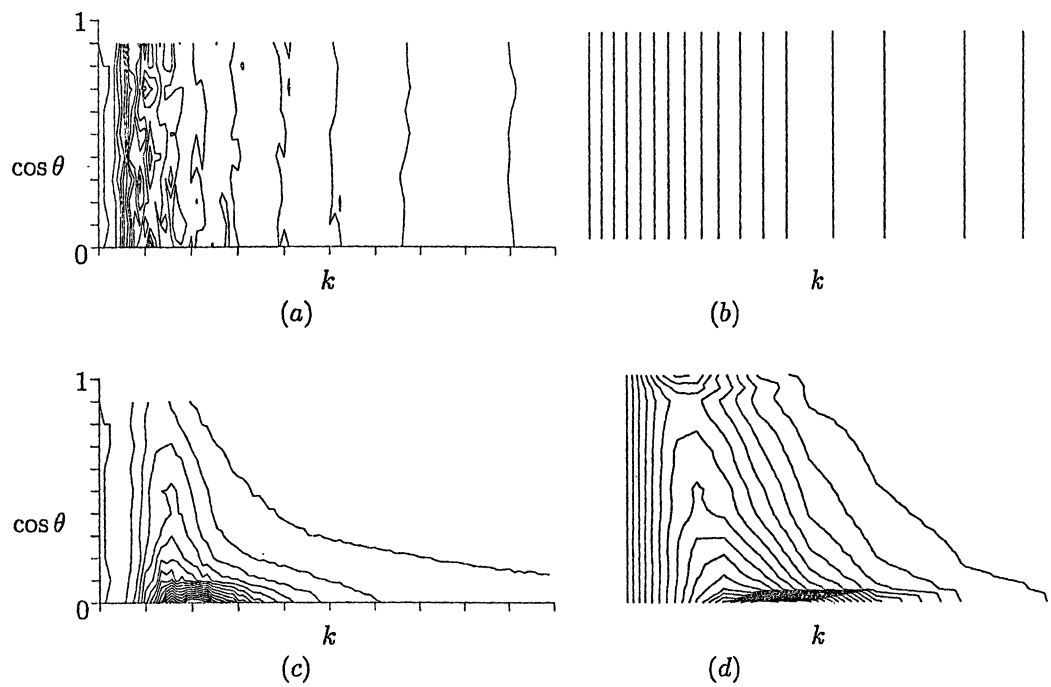

Figure 3. Isolines of turbulent kinetic energy $e(k, \cos\theta_k, t)$ for LES computations: (a) at $\Omega = 0$ at time $t/\tau = 427$; (b) EDQNM2 with $\Omega = 0$; (c) LES with $\Omega = 1$ at $t/\tau = 575$; and (d) EDQNM2 calculation with $\Omega = 1$ at time $t/\tau = 148$. The vertical axis bears $\cos\theta_k$ (from 0 to 1 upwards) and the horizontal one the wave number k. See Cambon et al. [19].

4. Additional role of forcing and solid walls

Although they confirm the significant anisotropisation linked to partial two-dimensionalisation, high resolution DNS and LES of unforced, initially 3D isotropic, rotating turbulence do not really show creation of coherent quasi-2D vortices, as far as the conditions for reproducing homogeneity are fulfilled. One of these conditions is to stop the computation when the most amplified integral lengthscale becomes of the same order of magnitude as the length of the computational box. A good compromise to reach higher elapsed times without developing spurious anisotropy was obtained by Mansour with an elongated computational box with length in axial direction four times the length in other two directions (corresponding to $512 \times 128 \times 128$ LES used in Cambon et al. [19]). Apparently more complete two-dimensionalisation with creation of strong axial rotors was shown in the low resolution 64^3 LES of Bartello et al. [28], but this seems to be a numerical artifact due to blocking the integral lengthscales when the computation is performed for too large elapsed times. Another difference of the latter study with DNS and LES studies, in which homogeneity is fulfilled (Bardina et al. [21], Cambon et al. [19]), was the rise in [28] of a two-component limit for the Reynolds stress tensor ($\langle u_3^2 \rangle \ll \langle u_1^2 \rangle \sim \langle u_2^2 \rangle$), in close connection with interference with periodic boundaries.

The last numerical study has suggested that boundary effects are important for reenforcing the rise of coherent axial vortices. Hence a numerical simulation of rotating turbulence between two solid parallel walls has been performed by Godeferd and Lollini [29] by means of a pseudo-spectral code. Another, more important, motivation for the DNS was to try to reproduce the essential results of the experiment by Hopfinger et al. [5] in which confinment and local forcing are additional, essentially inhomogeneous, effects with respect to the Coriolis force. Typical DNS results are briefly presented and discussed as follows.

A transition is shown to occur between the region close to the forcing and an outer region in which coherent vortices appear, the number of which depends on the Reynolds and Rossby numbers. Identification of vortices is shown in *figure 4* using both horizontal sections of iso-vorticity surfaces (noisy spots in the bottom plane of

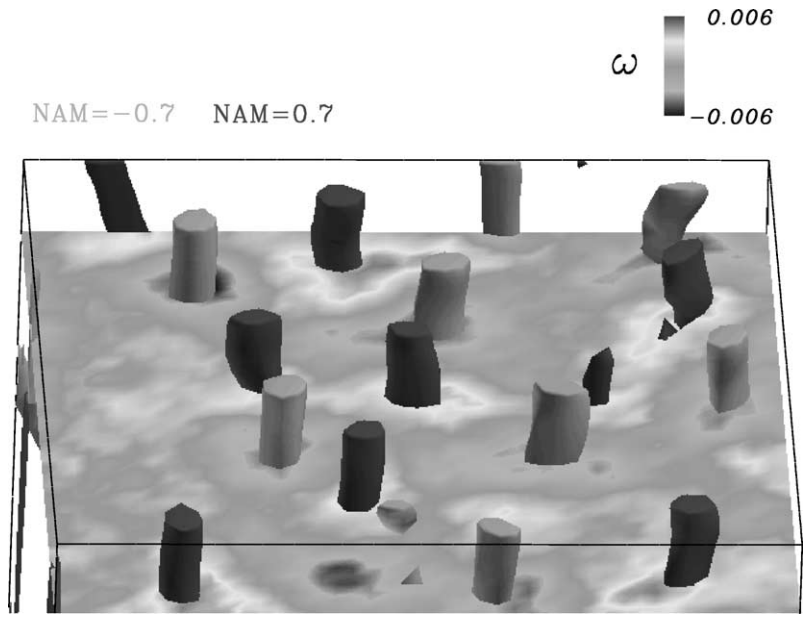

Figure 4. Vortex structures identified by NAM iso-values (tubes) and horizontal cross section of vorticity iso-values (noisy spots in the bottom plane). Courtesy Godeferd and Lollini [29]. NAM value at point M is obtained by averaging $|\mathbf{MP} \times \mathbf{u}(P)|/(|\mathbf{MP}||\mathbf{u}(P)|)$ over points P in a small domain surrounding M.

the figure) and isovalue surfaces of a normalized angular momentum, which is defined in the caption. The latter criterion (Normalized Angular Momentum) was suggested by experimentalists in PIV for obtaining smooth isovalues.

Asymmetry in terms of cyclones-anticyclones is mainly induced by the Ekman pumping near the solid boundaries, yielding helical trajectories. This is illustrated in *figure 5*, in which a pair cyclone-anticyclone is isolated. Even if the Ekman pumping generates a three-component motion, the presence of the horizontal walls, and the presence of the forcing in a horizontal plane between them, are essential for enforcing coherent vortices.

Nevertheless, and in contrast with the experimental results, no significant asymmetry cyclone-anticyclone was obtained in terms of number and intensity. In the same way, the typical distance between adjacent vortices is of the same order of magnitude as their diameter, and the Rossby number in their core is close to one. It was expected that for a given symmetric distribution of more intense and concentrated vortices (higher Rossby number), the centrifugal instability could act in destabilizing the anticyclones, so that dominant cyclones could emerge, as in the physical experiment. It seems that the insufficiently high Reynolds number is responsible for the lack of intensity and concentration. Hence, the conditions of stability – rediscussed in the conclusion section – are no relevant for strongly favouring the cyclonic eddies, but they could do that for higher Reynolds DNS or LES.

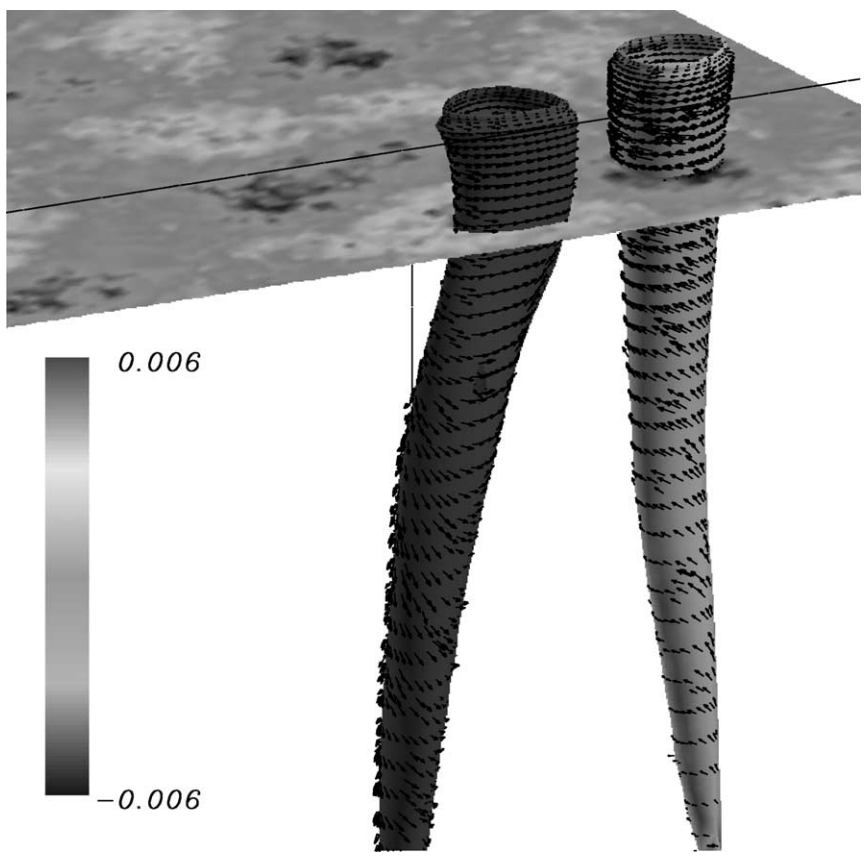

Figure 5. Selected pair of cyclonic-anticyclonic eddy structures, identified by NAM = 0.7 isosurfaces. Helical lines along them correspond to instantaneous streamlines in close vicinity of isosurfaces. Courtesy Godeferd and Lollini [29].

5. Pure stratified homogeneous turbulence

The case of stably stratified turbulence is very different, even if the gravity waves present strong analogies with inertial waves, and if almost all the equations of section 3 remain valid, changing only the definition of eigenmodes and dispersion relation, and extending the summation on the polarity index ε to $\varepsilon = 0$. An additional element is the presence of the 'vortex', or PV, mode, which is the steady linear mode and corresponds to $\varepsilon = 0$ in (10). According to the Craya–Herring decomposition, it is present for any wavevector orientation, and contains half the total kinetic energy in the isotropic case. Accordingly, pure vortex interactions were found to be dominant (resonant conditions are obtained with $\varepsilon = \varepsilon' = \varepsilon'' = 0$ in (10) with no need to restrict to resonant surfaces as for resonant wave interactions). EDQNM2 [13] and DNS results [30] have shown that the spectral energy concentrates towards vertical wavenumbers $k_\perp \sim 0$. These wavenumbers correspond to horizontally (because $\mathbf{k}$ and $\widehat{\mathbf{u}}$ are perpendicular) stratified turbulent structures with dominantly horizontal, low-frequency motions. As for the '2D transition' expected in pure rotation, a new dynamical insight is given to the collapse of vertical motion expected in stably stratified turbulence, but the long-time behaviour essentially differs from a 2D one.

A sketch of the different effects of pure rotation and pure stratification is shown in *figure 6*. Previous EDQNM ([31]) studies focused on triple correlations characteristic times modified by wave frequencies, whereas wave-turbulence theories proposed scaling laws for wave-part spectra. None of them, however, was capable of connecting wave-vortex dynamics to the vertical collapse and layering. Only recently, reintroducing a small but significant vortex part in their wave turbulence analysis, Caillol and Zeitlin [3] found that: "The vortex part obeys a limiting slow dynamics equation exhibiting vertical collapse and layering which may contaminate the wave-part spectra". This is in complete agreement with the main finding of [13]. It is important to point out that this result in [13] reflects a scrambling of any triadic interactions, like $(0, \pm 1, \pm 1)$, including at least one 'rapid'

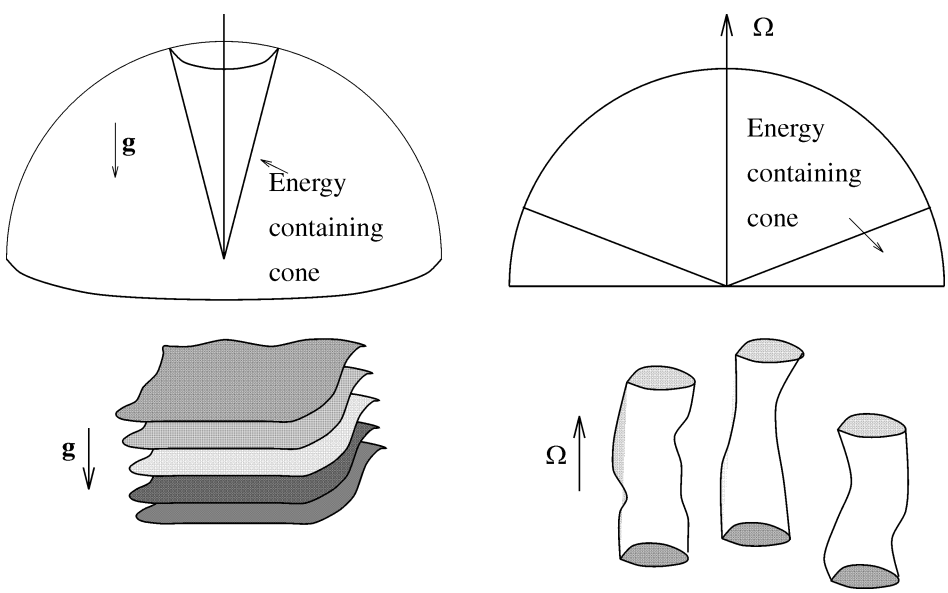

Representation of the spectral angular dependence occurring in stratified (top left) and rotating (top right) turbulence, with the corresponding schematic physical structures: layered flow (bottom left) for stratification; columnar vertically correlated shapes (bottom right) for rotation.

Figure 6. Sketch of the angular dependence of spectral energy occuring in stratified (top left) and rotating (top right) turbulence, with the corresponding shematic structures in physical space (bottom). See Godeferd and Cambon [13].

wave mode, so that the interaction which involves only slow modes becomes dominant. The corresponding energy transfer is strongly anisotropic in [13], it does not yield a classic cascade (which would contribute to dissipate the energy) but instead yields the angular drain of energy which condenses the energy towards vertical wave-vectors, in agreement with vertical collapse and layering. The subsequent angular dependent shape of the PV spectrum $\widehat{V}^{11}(k, \cos\theta_k, t)$, and total (kinetic + potential) energy spectrum $\widehat{V}^{ii}(k, \cos\theta_k, t)$ is illustrated by typical results from EDQNM2 and DNS [32,33]. Generalizing (19), $\widehat{V}^{ij}$ components are defined by

$$\left\langle \widehat{v}^{(i)*}(\mathbf{p}, t)\widehat{v}^{(j)}(\mathbf{k}, t)\right\rangle = \widehat{V}^{ij}(\mathbf{k}, t)\delta(\mathbf{k}-\mathbf{p}), \tag{28}$$

from $\widehat{v}^{(i)} = \widehat{\mathbf{v}}\cdot\mathbf{e}^{(i)}$, $i = 1, 2, 3$, 'including the direction' $\cos\theta_k = \pm 1$ (see Appendix and the remark below). Concentration of spectral total energy $E_{tot}(k, \cos\theta_k, t) = \widehat{V}^{ii}/(8\pi k^2)$ towards vertical wave vectors ($\theta_k \sim 0$) is illustrated by *figure 7*. The latter effect is reflected in physical space by the development of two different integral length scales, as shown in *figure 8*. $L_{11}^{(1)}$ is shown to develop similarly to isotropic unstratified turbulence, whereas $L_{11}^{(3)}$ is blocked. In the same conditions, with initial equipartition of potential and wave energy, linear calculation (RDT) exhibits no anisotropy, as stressed in section 2.

At much larger times, the transfer terms including wave contribution could become significant through resonant wave triads, as the Riley–Lelong $(0, \pm 1, 0)$ triads [10], but this would occur in a velocity field yet strongly altered by vertical collapse and layering. Very recently, concentration of kinetic energy towards vertical wave vectors and large scales was obtained by Smith and Waleffe [34] using high resolution DNS, which were forced randomly at small scale.

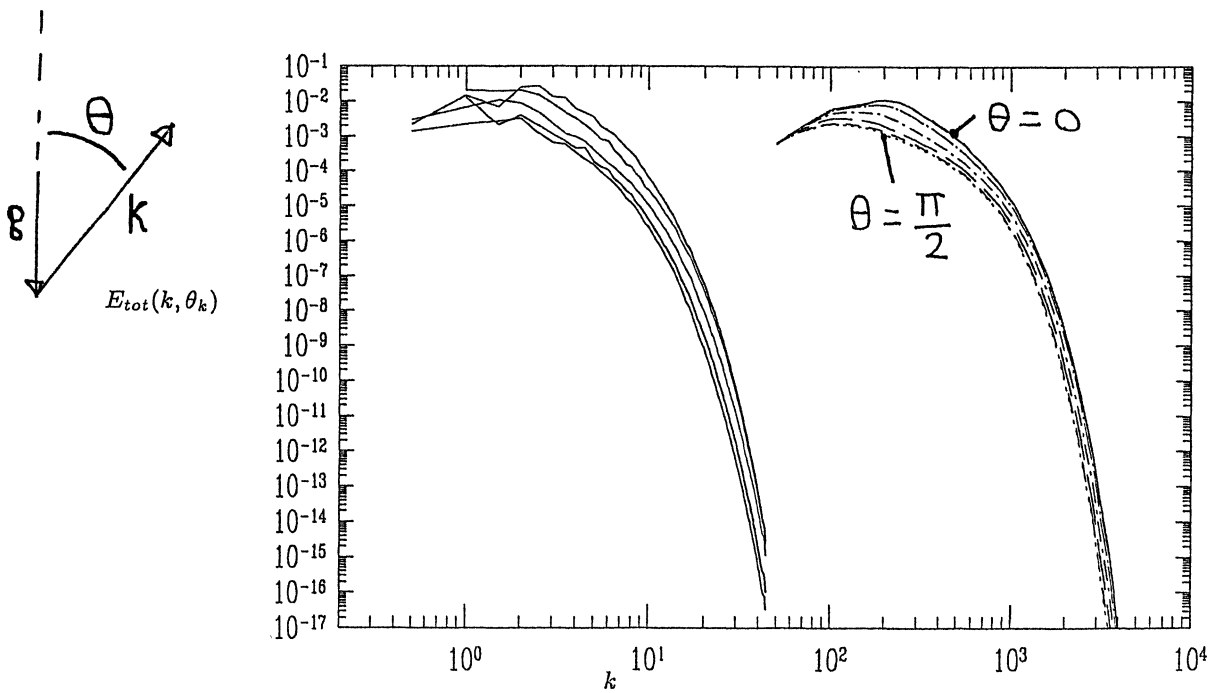

Figure 7. Typical angular dependence for total energy spectra $E_{tot}(k, \cos\theta_k, t)$, induced by stratification through nonlinear energy transfers, from 256^3 DNS (left) and EDQNM2 (right, shifted two decades to the right), started with the same purely isotropic initial data. $Nt/(2\pi) = 6$, $N = \pi/2$. The more energetic spectra (top curves) correspond to wave vectors close to the vertical direction, and the bottom spectra for the horizontal orientation of wavevectors. There are a total of 5 orientations in between for DNS, and 7 for EDQNM2, from $\cos\theta = 0$ to $\cos\theta = 1$ with a constant step. Courtesy Godeferd and Staquet [33].

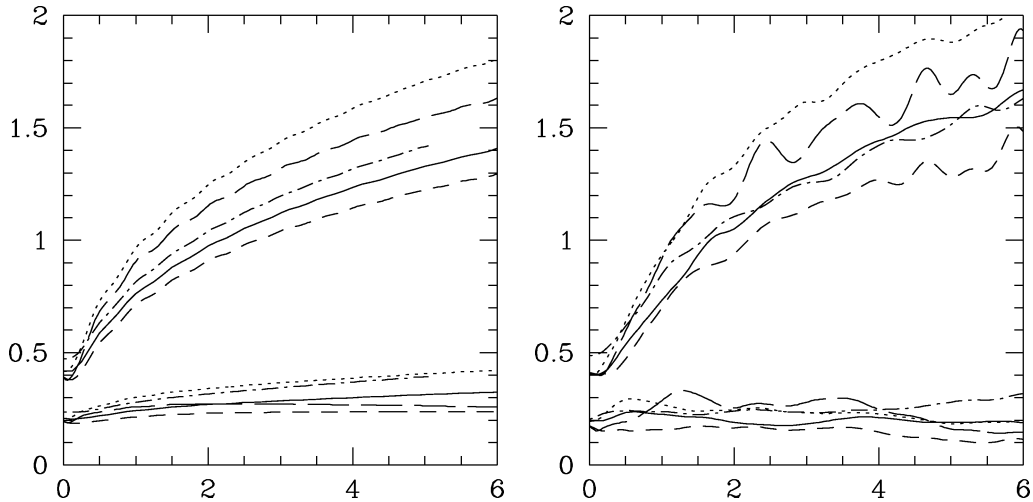

Figure 8. Development of integral length scales with horizontal ($L_{11}^{(1)}$, top values) and vertical ($L_{11}^{(3)}$, bottom values) separations, from EDQNM2 (left) and 256^3 DNS (right). Courtesy Godeferd and Staquet [32].

Remark: The mode related to vertical wave-vectors appears to be very important, since the concentration of spectral energy on it is the best identification for the development of vertical collapse and layering. It corresponds to the limit of the wavy mode, when the dispersion frequency tends to zero. Strictly speaking, this mode is a slow mode, which cannot be incorporated in the wave-vortex decomposition of Riley et al. [9], and more generally is not present in a classical poloidal–toroidal decomposition. It is absorbed in any decomposition based on the Craya–Herring frame (see Appendix), provided that some care be given to extend by continuity the definition of the unit vectors ($\mathbf{e}^{(1)}$, $\mathbf{e}^{(2)}$) towards $\mathbf{k} \parallel \mathbf{n}$ (Cambon [24], and Cambon et al. [35]). In so doing, the mode related to $\mathbf{e}^{(1)}$ coincides with a toroidal, or 'horizontal vortex', mode, but for vertical wave vectors, where it includes half the energy of the vertical slow mode. In the same way, the mode related to $\mathbf{e}^{(2)}$ coincides with a poloidal mode, affected by the wavy motion, but for vertical wave vectors, where it includes the other half of the energy of the vertical mode. In the different context of weaky nonlinear and weakly inhomogeneous RDT approach, and related DNS of Galmiche et al. [36], the vertical mode is considered as part of the mean flow and is called mean vertical shear mode (see Cambon et al. [35], for a general discussion and detailed comparison of different decompositions). In fact, the previous DNS works use Fourier modes and periodic boundary conditions in all directions, with initially injection of energy onto the largest vertical mode ($k_1 = k_2 = 0$, $k_3 = k_{\min}$), the so-called 'mean shear mode', so that their interpretation in terms of inhomogeneous turbulence and mean-fluctuating interaction is only a possible interpretation. More consistently, these results could be reinterpreted as purely homogeneous strongly anisotropic, illustrating concentration of energy towards vertical wave-vectors as in the theoretical and numerical works by Godeferd and Cambon [13], Godeferd and Staquet [32,33] and Smith and Waleffe [34].

6. Rotating and stratified turbulence

The general decomposition in terms of eigenmodes (Appendix) is valid in this case, as the main part of equations throughout this paper. The linear steady mode associated with $\varepsilon = 0$ in (10) is the quasi-geostrophic mode, whereas the two wavy modes ($\varepsilon = \pm 1$) are associated with inertio-gravity waves whose dispersion law is given by (7). In addition to the particular cases extensively discussed in the previous sections, the pure rotation

being somewhat singular, another special case has to be quoted: for $N = 2\Omega$, the dependency of the dispersion law on **k** vanishes, so that the group velocity is zero.

Even if analyses, such as wave-turbulence theory or statistical theory, for pure rotation and pure stratification can be generalized without problems of principle, one has to keep in mind two main characteristics as follows:

- the steady, or quasi-geostrophic mode, exists for all directions in wave-space, except if particular initial data have no projection onto it, and all triadic interactions $(0, 0, 0)$ are resonant;
- there is no 'slow' wavy mode, since the frequency given by (7) is never zero. This excludes resonance for Riley–Lelong triads of type $(0, \pm 1, 0)$.

Looking at numerical results, DNS of decaying turbulence from Kimura and Herring [37] illustrate different columnar or pancake-shape structures, according to rotation dominated or stratification dominated cases (*figure 9*). Quantitative results and detailed spectral analysis of DNS are in progress [18]. Both DNS and asymptotic models will be carried out and analysed in terms of the ratio $B = 2\Omega/N$, the Froude number, and the Reynolds number. The case of combined effects of rotation and stratification presents particular interest in the geophysical context for large enough horizontal length scales, and is the subject of many works in progress, using weakly nonlinear wave-turbulence theories and accurate DNS data. Theoretical investigation of pancake dynamics and geostrophic adjustment is performed by Babin et al. [1], in the case $BL_h/L_v \sim 1$, in which the ratio of horizontal to vertical lengthscale L_h/L_v is assumed large a priori. For unsteady flows dominated by stable stratification ($B \ll 1$), which are increasingly organised in thin pancakes, even a weak additional rotation seems to be a good candidate for inhibiting the decrease of the thickness of the layers – the pancake aspect ratio. The recent approach by Smith and Waleffe [34] using DNS with forcing from the small scales is one of the more promising, since the numerical method is based on a decomposition in terms of eigenmodes, similar to the one used in this paper, with investigation of energy concentration at larger scales (for instance $1/2$ of the forcing wavenumber without rotation) towards different modes and different wavevector orientations.

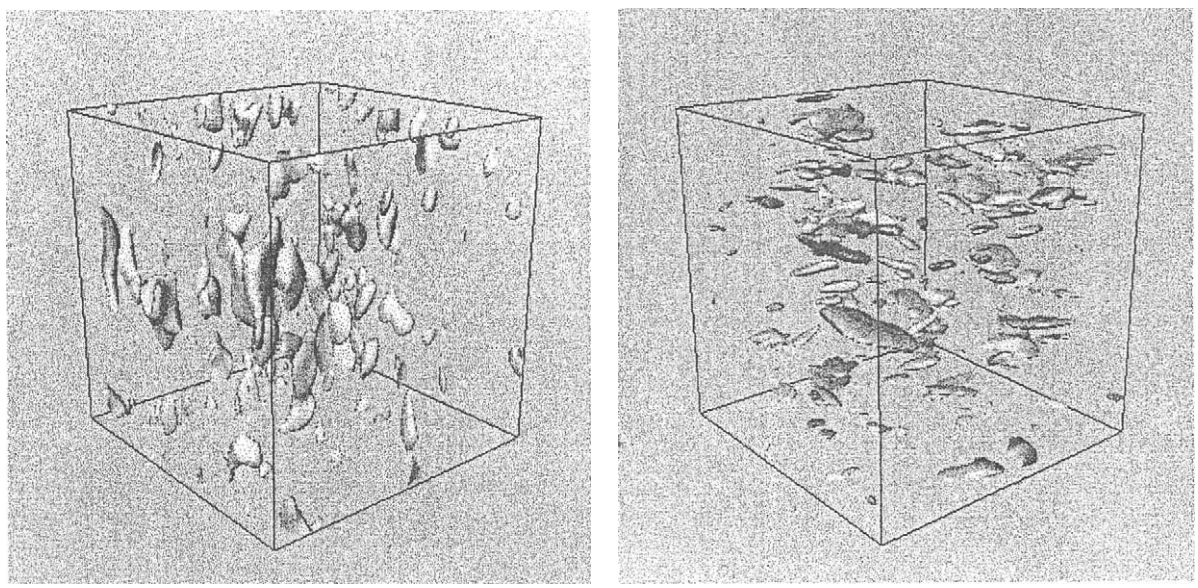

(a) (b)

Figure 9. Isovorticity surfaces from DNS calculations for (a) rotating, and (b) stratified turbulence. See [16]. Courtesy Kimura and Herring.

In particular, concentration towards vertical wavevectors is found for $B \ll 1$, whereas concentration towards horizontal wavevectors, preferentially for the 'vortex' mode, is found for $B \gg 1$.

7. Concluding comments and open problems

This subsection is organised in four items, which illustrate important contributions to the domain of models and description of homogeneous 'anisotropic' turbulence, the explicit role of confinment, and stability analyses of large scale vortices.

1. Anisotropic 'two-point closures' ([19,16]) versus 'wave-turbulence' theories ([1,2,4]).
   As for 'RDT' and 'linear stability' communities, there are too few common works on possible points of contact between the two communities. An important common formalism exists, provided the closures be using the bases of eigenmodes. The presence of a damping term in the closures, as μ_k in (26) plays a particular role, even if very small, to regularise the 'resonance operator', which often reduces to a Dirac Delta function in wave-turbulence theories [22]. Note that simple results for scaling of Kolmogorov spectra were obtained in wave turbulence theory with pure isotropic dispersion laws as $\sigma_k = |\mathbf{k}|^\alpha$, assuming constant isotropic spectral energy flux [4]. Such procedures are excluded in all the highly anisotropic cases reported in this paper, in which the angular drain of energy in spectral space is shown to be dominant with respect to the classic cascade mediated by isotropic fluxes.
2. Anisotropy versus structure.
   Anisotropic spectral description, with angular dependence of spectra and cospectra in Fourier space, allows to quantify columnar or pancake structuring in physical space. Among various indicators of the thickness and width of pancakes, which can be readily derived from anisotropic spectra, integral lengthscales $L_{ij}^{(l)}$ related to different components and orientations are the most useful.
   As another illustration ([38,39]), the streaklike tendency in a shear flow can be easily found in calculating both the $L_{11}^{(1)}$ component, which gives the streamwise length of the streaks, and $L_{11}^{(3)}$, which gives the spanwise separation length of the streaks (as usual, 1 and 3 reffer to streamwise and spanwise coordinates, respectively). In pure homogeneous RDT at constant shear rate, both length scales can be calculated analytically and their ratio (elongation parameter) is found to increase as $(St)^2$, $S = \partial U_1/\partial x_2$ being the shear rate.
   As a final comment about anisotropy, I would like to underline that a fully anisotropic spectral (or two-point) description carries out a very large amount of information, even if it only concerns second-order statistics. In the inhomogeneous case, the pod (proper orthogonal decomposition) has renewed the interest for second-order two-point statistics [40], but this technique is never applied completely in the homogeneous 'anisotropic' case. It is only said that pod spatial modes are Fourier modes in the homogeneous case, but the true spectral eigenvectors corresponding to pod modes are not considered. This can be obtained in diagonalizing the tensor Φ_{ij}, and is an easy task using the above $e - Z$ decomposition (20)–(21) (the angular position of the principal axes, which are associated with the nonzero principal components $e + |Z|$ and $e - |Z|$, is fixed by the phase of Z, at each $\mathbf{k}$).
3. Homogeneous versus confined turbulence.
   Vertical confinement and local forcing were shown to favour the emergence of organised eddies, in the rotating flow, even if the Ekman layer and the forcing generated more three-dimensionality at small scale. More generally, interaction of walls with the 'natural' development of columnar/pancake structures has to be studied in the general case. The case of turbulence in flattened boxes with periodic boundary conditions, when the aspect ratio is not in agreement with this 'natural' tendency, is outside the domain of homogeneous turbulence, and is not discussed in this paper.

4. Structure versus stability analysis.
   This topic may link our survey of rotating flows to the stability analysis of preexisting coherent vortices (see Klosterziel and van Heijst [41], and Cambon [42], for a recent survey). However, the vortices appearing in *figure 6* seem to be too weak to be affected by the centrifugal and/or elliptic instabilities discussed in Cambon [42], so that a clear asymmetry in terms of cyclonic and anticyclonic eddies was not found. For the stably stratified case, a recent 'zig-zag' instability (Billant and Chomaz [43]) was recently proposed to explain the layering (see also Dritschel et al. [44], in the different context of quasi-geostrophic flows with both stable stratification and system rotation). The typical thickness of the slices, however, is likely much larger than the one seen in a typical turbulent stratified flow (see Garrett and Munk [45]). Even if linear stability of preexisting large coherent structures can give qualitative information about the geometry of columnar/pancakes fine structures, nonlinear (and nonisotropic) cascade and dissipation remains essential features to predict typical length scales.

Appendix: Eigenmode decomposition

The notations are mainly the same as in Godeferd and Cambon [13]. The fluctuating field for both velocity u_i and temperature τ is gathered into a unique 3D vector v_i, as in (8). The Fourier coefficients for its 3 components in the fixed frame of reference are $(\widehat{v}_i, i = 1, 2, 3)$ with 3 the vertical direction. They become $\widehat{v}^{(i)}$ in the Craya–Herring local frame of reference $(\mathbf{e}^{(1)}, \mathbf{e}^{(2)}, \mathbf{e}^{(3)})$, whose definition – direct orthonormal – is recalled below.

$$\mathbf{e}^{(1)} = \frac{\mathbf{k}\times\mathbf{n}}{|\mathbf{k}\times\mathbf{n}|}, \qquad \mathbf{e}^{(2)} = \frac{\mathbf{k}}{k}\times\mathbf{e}^{(1)}, \qquad \mathbf{e}^{(3)} = \frac{\mathbf{k}}{k}. \tag{29}$$

Consequently, the unit vectors $\mathbf{e}^{(1)}$ and $\mathbf{e}^{(2)}$ lie in the plane orthogonal to $\mathbf{k}$, such that $\mathbf{e}^{(1)}$ is normal to the polar axis $\mathbf{n}$. They exactly correspond to toroidal and poloidal modes in physical space. Their definition (29) is not valid for pure vertical wave-vectors, or $|\mathbf{k}\times\mathbf{n}| = k_\perp = 0$, and has to be completed for this case [24, 35]. For $k_\perp = 0$, $(\mathbf{e}^{(1)}, \mathbf{e}^{(2)})$ may coincide with any direct orthonormal frame of reference in the horizontal plane, $\mathbf{k} \perp \mathbf{n}$, and the specification of the azimutal angle to fix it in this plane depends on the problem. This angle is unimportant when two-point statistics are addressed, with the additional constraint of statistical axisymmetry. For the latter symmetry, which is preserved by background equations if satisfied by initial data, the spectral tensor defined in (28) reduces to five nonzero real components, $\widehat{V}^{11}$, $\widehat{V}^{22}$, $\widehat{V}^{33}$ being real, and $\widehat{V}^{23}$ being complex, all of them depending on $(k, \cos\theta_k, t)$. The density of kinetic energy is recovered as $e = (1/2)(\widehat{V}^{11} + \widehat{V}^{22})$, with necessary equipartition for vertical wavevectors $\widehat{V}^{11}(k, \pm 1, t) = \widehat{V}^{22}(k, \pm 1, t)$. The latter condition, together with $\widehat{V}^{23}(k, \pm 1, t) = 0$, or polar isotropy, allows us to get rid of the azimutal angle of the local frame $(\mathbf{e}^{(1)}, \mathbf{e}^{(2)})$ when extending its definition to $\cos\theta_k = \pm 1$.

From the velocity and vorticity Fourier modes in the local frame, or

$$\widehat{\mathbf{u}} = \widehat{u}^{(1)}\mathbf{e}^{(1)} + \widehat{u}^{(2)}\mathbf{e}^{(2)}, \qquad \widehat{\boldsymbol{\omega}} = \imath k\big(\widehat{u}^{(1)}\mathbf{e}^{(2)} - u^{(2)}\mathbf{e}^{(1)}\big), \tag{30}$$

is derived

$$\widehat{u}^{(1)} = \imath\frac{\widehat{\omega}_\parallel}{k_\perp}, \qquad \widehat{u}^{(2)} = -\frac{k}{k_\perp}\widehat{u}_\parallel, \tag{31}$$

with $k_\perp = |\mathbf{k}\times\mathbf{n}|$. According to the general definition (8) of $\widehat{\mathbf{v}}$, $\widehat{v}^{(1)} = \widehat{u}^{(1)}$, $\widehat{v}^{(2)} = \widehat{u}^{(2)}$, and the rescaled buoyancy force is connected to the third component as

$$\widehat{v}^{(3)} = \mathbf{e}^{(3)}\cdot\widehat{\mathbf{v}} = \imath N^{-1}\widehat{b}. \tag{32}$$

Note that the three-component term denoted $\mathbf{W}_k$ (Bartello [46], Riley and Lelong [10], p. 626) is closely linked to $\widehat{\mathbf{v}}$ through $W_1 = -\imath\,\widehat{v}^{(1)}$, $W_2 = +\imath\,\widehat{v}^{(2)}$, $W_3 = -\imath\,\widehat{v}^{(3)}$, but cannot be interpreted as a true vector (a definition of an inverse reference frame of type (29), however, would give a strict proportionality of $\mathbf{W}_k$ and $\widehat{\mathbf{v}}$ components, as pointed out by one referee). Anyway $\widehat{\mathbf{v}}$ has many advantages, being a true vector defined independently of the reference frame, even for $\mathbf{k} \parallel \mathbf{n}$, and $\mathbf{v}$ is a real vector in physical space, due to Hermitian property of (8).

In the local (Craya–Herring) frame, the linearized system of equations (1)–(3) becomes:

$$\partial_t \begin{pmatrix} \widehat{v}^1 \\ \widehat{v}^2 \\ \imath\widehat{v}^3 \end{pmatrix} + \begin{pmatrix} 0 & -\sigma_r & 0 \\ \sigma_r & 0 & -\sigma_s \\ 0 & \sigma_s & 0 \end{pmatrix} \begin{pmatrix} \widehat{v}^1 \\ \widehat{v}^2 \\ \imath\widehat{v}^3 \end{pmatrix} = 0 \tag{33}$$

or $\partial_t \widehat{\mathbf{v}} + M\widehat{\mathbf{v}} = 0$, where

$$\sigma_r = 2\Omega\cos\theta, \qquad \sigma_s = N\sin\theta, \qquad \sigma = \sqrt{\sigma_r^2 + \sigma_s^2} \tag{34}$$

are respectively the absolute value of dispersion law frequencies for inertial waves, gravity waves, and inertio-gravity waves.

The system of equations (33) is easily solved by diagonalizing the matrix M. Three eigenmodes are obtained in the local frame as follows:

$$\mathbf{N}^0 = \begin{pmatrix} \sigma_s/\sigma \\ 0 \\ \sigma_r/\sigma \end{pmatrix}, \qquad \mathbf{N}^1 = (\sqrt{2}/2) \begin{pmatrix} -\sigma_r/\sigma \\ \imath \\ \sigma_s/\sigma \end{pmatrix}, \qquad \mathbf{N}^{-1} = (\sqrt{2}/2) \begin{pmatrix} -\sigma_r/\sigma \\ -\imath \\ \sigma_s/\sigma \end{pmatrix}. \tag{35}$$

They are related to the eigenvalues 0, $+\sigma$ and $-\sigma$, respectively. $\mathbf{N}^0$ is the stationary mode, which coincides with the quasi-geostrophic mode QG; it comprises two contributions, one from the horizontal divergencefree velocity mode $\mathbf{e}^{(1)}$ ('vortex' mode), and one from the mode $\mathbf{e}^{(3)}$ associated with the temperature field. $\mathbf{N}^{\pm 1}$ are the 'wavy' modes, called ageostrophic modes hereinafter in agreement with classic geophysical literature. They do not exactly coincide with corresponding modes defined in the particular case of pure rotation [19] or pure stratification [13], up to normation coefficients ($\imath$, $-\imath$, $\sqrt{2}$, ...). The wave-vortex terminology was used by Riley et al. [9] for analysis of DNS of stably stratified turbulence, and in a more geophysically related context, the geostrophic and ageostrophic counterparts, by Bartello [46] and Babin et al. [1]. (See also Leith [47], and the recent annual review by Riley and Lelong [10].)

The basis of eigenmodes is used to express $\widehat{\mathbf{v}}$ as

$$\widehat{\mathbf{v}} = \sum_{\varepsilon=0,\pm1} \xi^{\varepsilon} \mathbf{N}^{\varepsilon}, \tag{36}$$

with

$$\xi^{\varepsilon} = \widehat{\mathbf{v}} \cdot \mathbf{N}^{-\varepsilon}, \quad \varepsilon = 0, \pm 1, \tag{37}$$

in agreement with simple relationship for scalar products $\mathbf{N}^{\varepsilon} \cdot \mathbf{N}^{-\varepsilon'} = \delta_{\varepsilon\varepsilon'}$. Accordingly, the initial value ($t = 0$) linearised system of equations (1)–(3) has a general solution as follows:

$$\widehat{\mathbf{v}}(\mathbf{k}, t) = \sum_{\varepsilon=0,\pm1} \mathbf{N}^{\varepsilon} \mathrm{e}^{-\imath\varepsilon\sigma t} \left[\mathbf{N}^{-\varepsilon} \cdot \widehat{\mathbf{v}}(\mathbf{k}, 0)\right]. \tag{38}$$

Acknowledgments

Stimulating discussions with George Carnevale, Martin Galmiche, Fabien Godeferd, Robert Rubinstein and Leslie Smith are reflected in this paper. In addition, the initial manuscript was significantly improved through clear and concise comments by both referees.

References

[1] Babin A., Mahalov A., Nicolaenko B., On the nonlinear baroclinic waves and adjustment of pancake dynamics, Theor. Comput. Fluid Dynamics 11 (1998) 215–235.
[2] Benney D.J., Saffman P.G., Nonlinear interactions of random waves in a dispersive medium, Proc. R. Soc. London Ser. A 289 (1966) 301–320.
[3] Caillol P., Zeitlin W., Kinetic equations and stationary energy spectra of weakly nonlinear internal gravity waves, Dyn. Atm. Oceans 32 (2000) 81–112.
[4] Zakharov V.E., L'vov V.S., Falkowich G., Kolmogorov Spectra of Turbulence. I. Wave Turbulence, Springer Series in Nonlinear Dynamics, Springer-Verlag, 1992.
[5] Hopfinger E.J., Browand F.K., Gagne Y., Turbulence and waves in a rotating tank, J. Fluid Mech. 125 (1982) 505.
[6] Mowbray D.E., Rarity B.S.H., A theoretical and experimental investigation of the phase configuration of internal waves of small amplitude in a density stratified liquid, J. Fluid Mech. 28 (1967) 1–16.
[7] Lollini L., Thèse de Doctorat, Université Lyon 1, France, 1997.
[8] Greenspan H.P., The Theory of Rotating Fluids, Cambridge University Press, 1968.
[9] Riley J.J., Metcalfe R.W., Weisman M.A., DNS of homogeneous turbulence in density stratified fluids, in: West B.J. (Ed.), Proc. AIP Conf. on Nonlinear Properties of Internal Waves, AIP, New York, 1981, pp. 79–112.
[10] Riley J.J., Lelong M.-P., Fluid motions in the presence of strong stable stratification, Annu. Rev. Fluid Mech. 32 (2000) 613–657.
[11] Craya A., Contribution à l'analyse de la turbulence associée à des vitesses moyennes, P.S.T. n° 345, Ministère de l'air, France, 1958.
[12] Cambon C., Spectral Approach to Axisymmetric Turbulence in a Stratified Fluid, Advances in Turbulence 2, Springer-Verlag, Berlin, 1989.
[13] Godeferd F.S., Cambon C., Detailed investigation of energy transfers in homogeneous stratified turbulence, Phys. Fluid 6 (1994) 2084–2100.
[14] van Haren L., Thèse de Doctorat, Université Lyon 1, France, 1993.
[15] Hanazaki H., Hunt J.C.R., Linear processes in unsteady stably stratified turbulence, J. Fluid Mech. 318 (1996) 303–337.
[16] Cambon C., Scott J.F., Linear and nonlinear models of anisotropic turbulence, Annu. Rev. Fluid Mech. 31 (1999) 1–53.
[17] Kaneda Y., Ishida T., Suppression of vertical diffusion in strongly stratified turbulence, J. Fluid Mech. 402 (2000) 311–327.
[18] Godeferd F.S., Cambon C., Nonlinear structuring effects in rotating stably stratified flows, in: 1st Symp. on TSFP, Santa Barbara, September 13–16, 1999.
[19] Cambon C., Mansour N.N., Godeferd F.S., Energy transfer in rotating turbulence, J. Fluid Mech. 337 (1997) 303–332.
[20] Jacquin L., Leuchter O., Cambon C., Mathieu J., Homogeneous turbulence in the presence of rotation, J. Fluid Mech. 220 (1990) 1–52.
[21] Bardina J., Ferziger J.M., Rogallo R.S., Effect of rotation on isotropic turbulence: computation and modelling, J. Fluid Mech. 154 (1985) 321–326.
[22] Rubinstein R., Double resonances and spectral scaling in the weak turbulence theory of rotating and stratified turbulence, ICASE report, 1999.
[23] Smith L.M., Waleffe F., Transfer of energy to 2D large scales in forced, rotating 3D turbulence, Phys. Fluids 11 (6) (1999) 1608–1622.
[24] Cambon C., Etude spectrale d'un champ turbulent incompressible soumis à des effets couplés de déformation et de rotation imposés extérieurement, Thèse de Doctorat d'État, Université de Lyon, France, 1982.
[25] Waleffe F., Inertial transfers in the helical decomposition, Phys. Fluid A 5 (1993) 677–685.
[26] Batchelor G.K., The Theory of Homogeneous Turbulence, Cambridge University Press, Cambridge, 1953.
[27] Godeferd F.S., Scott J.F., Cambon C., Asymptotic models for slow dynamics and anisotropic structure of turbulence in a rotating fluid, in: Dopazo C. (Ed.), Advances in Turbulence VIII, 2000, p. 981.
[28] Bartello P., Métais O., Lesieur M., Coherent structures in rotating three-dimensional turbulence, J. Fluid Mech. 273 (1994) 1–29.
[29] Godeferd F.S., Lollini L., Direct numerical simulations of turbulence with confinment and rotation, J. Fluid Mech. 393 (1999) 257–307.
[30] Godeferd F.S., Malik N.A., Cambon C., Nicolleau F., Eulerian and Lagrangian statistics in homogeneous stratified flows, Appl. Sci. Res. 57 (3–4) (1997) 319–335.
[31] Carnevale G.F., Martin P.C., Fields theoretical techniques in statistical fluid dynamics, with application to nonlinear wave dynamics, Geophys. Astrophys. Fluid Dyn. 20 (1982) 131.
[32] Godeferd F.S., Staquet C., Large and small scales anisotropy in stably stratified homogeneous turbulence, in: Developments in Geophysical Turbulence, NCAR, Boulder, June 16–19, 1998.
[33] Godeferd F.S., Staquet C., Statistical modelling and DNS of decaying stably-stratified turbulence: Part 2. Large and small scales anisotropy, J. Fluid Mech. (2000), submitted.
[34] Smith L.M., Waleffe F., Generation of slow, large scales in forced rotating, stratified turbulence, J. Fluid Mech. (2001), to appear.
[35] Cambon C., Galmiche M., Thual O., Optimal decomposition of motions in stably stratified fluids, Internal report, 2000.

[36] Galmiche M., Hunt J.C.R., Thual O., Bonneton P., Turbulence-mean field interactions and layer formation in a stratified fluid, Eur. J. Mech. B-Fluids 20 (4) (2001).
[37] Kimura Y., Herring J.R., Private communication, 1999.
[38] Lee J.M., Kim J., Moin P., Structure of turbulence at high shear rate, J. Fluid Mech. 216 (1990) 561–583.
[39] Salhi A., Cambon C., An analysis of rotating shear flows using linear theory and DNS and LES results, J. Fluid Mech. 347 (1997) 171–195.
[40] Lumley J.L., The structure of inhomogeneous turbulent flows, in: Yaglom A.M., Tatarski V.I. (Eds.), Atmospheric Turbulence and Radio Wave Propagation, Nauka, Moscow, 1967, pp. 166–167.
[41] Kloosterziel R.C., van Heijst G.J.F., An experimental study of unstable barotropic vortices in a rotating fluid, J. Fluid Mech. 223 (1991) 1–24.
[42] Cambon C., Stability of vortex structures in a rotating frame, in: Hunt J.C.R., Vassilicos J.C. (Eds.), Turbulence and Vortex Dynamics, Cambridge University Press, 2000, pp. 244–268.
[43] Billant P., Chomaz J.M., Experimental evidence for a new instability of a vertical columnar vortex pair in a strongly stratified fluid, J. Fluid Mech. 18 (2000) 167–188.
[44] Dritschel D.G., de la Torre Juárez M., Ambaum M.H.P., The three-dimensional vortical nature of atmospheric and oceanic turbulent flows, Phys. Fluids 11 (6) (1999) 1512–1520.
[45] Garrett C.J.R., Munk W.H., Internal waves in the ocean, Annu. Rev. Fluid Mech. 11 (1979) 339–369.
[46] Bartello P., Geostrophic adjustment and inverse cascades in rotating stratified turbulence, J. Atmos. Sci. 52 (1995) 4410–4428.
[47] Leith, C.E., Nonlinear normal mode initialization and quasi-geostrophic theory, J. Atmos. Sci. 37 (1980) 958–968.